An examination of multiplicity of steady states for two- and four-sided lid-driven cavity flows through an HOC scheme

†Chitrarth Prasad[1] and *Anoop K. Dass[2]

[1]Department of Mechanical Engineering, Indian Institute of Technology Guwahati, India
[2]Department of Mechanical Engineering, Indian Institute of Technology Guwahati, India

*Presenting author: anoop@iitg.ernet.in
†Corresponding author: chitrarth2009@gmail.com

Abstract

This work is concerned with the computation of two- and four-sided lid-driven cavity flows using a transient higher-order compact (HOC) scheme. The multiplicity of steady states for most of these configurations through the use of non-compact schemes is well known. In this work, these cases are re-examined using a spatially fourth- and a temporally second-order compact scheme. The threshold values of certain parameters such as the cavity aspect ratio (A) and the flow Reynolds number (Re) are also computed beyond which there is multiplicity of solutions. It is observed that for the motion of non-facing walls of a square cavity, multiple solutions can be obtained for $Re = 975$, which is significantly lower than the previously established value. For all the other cases, these critical values of parameters are in good agreement with the existing investigations. Multiple solutions are also obtained for antiparallel wall motion in two-sided square cavities, which do not feature in any of the previous investigations using non-compact schemes.

Keywords: lid-driven, higher-order compact, Reynolds number, aspect ratio

1 Introduction

Over the years the single lid-driven cavity flow has been used as a benchmark problem to test the performance of numerical schemes and algorithms for incompressible flows. The problem has attracted researchers because it contains a wide variety of interesting phenomenon in the simplest of geometric settings. The single lid-driven cavity flow was extended to two- and four-sided cavity flows by various investigators [1, 2, 3, 4, 5, 6, 7, 8, 9, 10], who observed that a plethora of vortex patterns can be generated with different aspect ratios and directions of motion of the walls.

It is well known that many nonlinear problems exhibit multiple steady solutions even though the governing equations and boundary conditions remain the same. As the governing equations for fluid flow are nonlinear in nature, the possibility of multiple solutions exists. Many researchers have found multiple solutions for parallel wall motion of facing walls for both rectangular and square cavities, and for antiparallel wall motion for rectangular cavities [1, 2, 3, 4, 5, 6, 7, 8, 9, 10]. Albensoeder et al. [2] were among the first to investigate the nonlinear regime and find multiple 2D steady states in rectangular two-sided lid-driven cavities. They have found upto five different flow states for both parallel and antiparallel motion of facing walls. Very recently Lemée et al. [6] addressed the issue of multiple solutions in square cavity with parallel motion of facing walls and found out a critical Reynolds number above which multiple solutions exist, which is consistent with [2]. Similar investigations have been carried out for two-sided cavities with motion of non-facing walls and for four-sided cavities [1, 8]. All these existing

investigations have been carried out using non-compact schemes. It can be observed from these investigations, that the additional solutions, if they exist, always exist in pairs.

In this work, we re-examine these solutions using a higher-order compact (HOC) scheme of spatially fourth- and temporal second-order accuracy. This scheme was developed by Kalita et. al [11] by differentiating the governing equation to obtain compact approximations for the leading truncation error terms. Grid independent results are carefully computed so that the results can be used as means to test other schemes and algorithms. For the two-sided rectangular cavity, computations are carried out at a fixed Reynolds number (Re) of 600 at various aspect ratios (A) for parallel motion of facing walls. It is seen that at $Re = 600$ multiple solutions exist only above a critical aspect ratio of 0.556. This value is very close to the value 0.559 reported in [2]. Computations are also carried out for square cavities having antiparallel and parallel motion of facing walls at various Re's. For parallel wall motion in a square cavity, a threshold value of $Re = 983.5$ is observed below which only stable symmetric solutions exist. This value is in good agreement with previously reported values in [2, 6]. For antiparallel motion of facing walls in a square cavity, till very recently, existence of multiple steady solutions was not experienced. In a recent communication [12], using the same HOC scheme as the one used here, we demonstrate that existence. This shows the accuracy and effectiveness of the present scheme, which we use here to compute multiple solutions for the motion of nonfacing walls in two- and four-sided configurations as well. It is observed that the limiting value of Re for four-sided cavity is very close to previously reported value in [8], however for motion of non-facing walls in two-sided cavity, multiple solutions are seen to exist even for $Re = 975$, which is significantly lower than the previously reported threshold value of 1071 [8].

This paper is organized in five sections. Section 2 describes the HOC scheme formulation and associated descritization. In Section 3 the credibility of the present HOC code is established through a comparison exercise with the results of a previously known benchmark work [13]. Section 4 presents the results and discussion. Concluding remarks are made in Section 5.

2 Scheme formulation

There have been various attempts at developing HOC schemes [14, 11, 15, 16, 17]. The scheme used in this work was developed by Kalita et al. [11]. We present here a brief description of their HOC scheme formulation.

The unsteady 2D transport equation for a general variable ϕ in some continuous domain with suitable boundary conditions can be written as

$$a\frac{\partial \phi}{\partial t} - \nabla^2 \phi + c(x,y,t)\frac{\partial \phi}{\partial x} + d(x,y,t)\frac{\partial \phi}{\partial y} = g(x,y,t) \tag{1}$$

where a is const, c and d are convection coefficients and g is forcing function. We take the steady state form of equation (1), which is obtained when ϕ,c,d and g are independent of t.

$$-\nabla^2 \phi + c(x,y)\frac{\partial \phi}{\partial x} + d(x,y)\frac{\partial \phi}{\partial y} = g(x,y) \tag{2}$$

Discretization with second-order central differencing on a uniform grid with spacing h and k in the $x-$ and $y-$directions respectively yields

$$-\delta_x^2 \phi_{ij} - \delta_y^2 \phi_{ij} + c\delta_x \phi_{ij} + d\delta_y \phi_{ij} - \tau_{ij} = g_{ij} \tag{3}$$

where ϕ_{ij} denotes $\phi(x_i, y_j)$; δ_x, δ_x^2 and δ_y, δ_y^2 are the first and second-order central difference operators along $x-$ and $y-$directions respectively. The truncation error τ_{ij} is given by

$$\tau_{ij} = \left[\frac{h^2}{12}\left(2c\frac{\partial^3\phi}{\partial x^3} - \frac{\partial^4\phi}{\partial x^4}\right) + \frac{k^2}{12}\left(2d\frac{\partial^3\phi}{\partial y^3} - \frac{\partial^4\phi}{\partial y^4}\right)\right] + O(h^4, k^4) \tag{4}$$

In order to obtain a fourth-order compact formulation for equation (2), each of the derivatives of the leading term in equation (4) are compactly approximated to $O(h^2, k^2)$. In order to do this the original PDE (2) is differentiated to yield expressions for higher derivatives. After these substitutions (3) yields [11]

$$\begin{aligned} &-\alpha_{ij}\delta_x^2\phi_{ij} - \beta_{ij}\delta_y^2\phi_{ij} + C_{ij}\delta_x\phi_{ij} + D_{ij}\delta_y\phi_{ij} \\ &-\frac{h^2+k^2}{12}\left[\delta_x^2\delta_y^2 - c_{ij}\delta_x\delta_y^2 - d_{ij}\delta_x^2\delta_y - \gamma_{ij}\delta_x\delta_y\right]\phi_{ij} = G_{ij} \end{aligned} \tag{5}$$

where the coefficients $\alpha_{ij}, \beta_{ij}, \gamma_{ij}, C_{ij}, D_{ij}, G_{ij}$ are as follows

$$\alpha_{ij} = 1 + \frac{h^2}{12}\left(c_{ij}^2 - 2\delta_x c_{ij}\right) \tag{6}$$

$$\beta_{ij} = 1 + \frac{k^2}{12}\left(d_{ij}^2 - 2\delta_y d_{ij}\right) \tag{7}$$

$$\gamma_{ij} = \frac{2}{h^2+k^2}\left(h^2\delta_x d_{ij} + k^2\delta_y c_{ij}\right) - c_{ij}d_{ij} \tag{8}$$

$$C_{ij} = \left[1 + \frac{h^2}{12}(\delta_x^2 - c_{ij}\delta_x) + \frac{k^2}{12}(\delta_y^2 - d_{ij}\delta_y)\right]c_{ij} \tag{9}$$

$$D_{ij} = \left[1 + \frac{h^2}{12}(\delta_x^2 - c_{ij}\delta_x) + \frac{k^2}{12}(\delta_y^2 - d_{ij}\delta_y)\right]d_{ij} \tag{10}$$

$$G_{ij} = \left[1 + \frac{h^2}{12}(\delta_x^2 - c_{ij}\delta_x) + \frac{k^2}{12}(\delta_y^2 - d_{ij}\delta_y)\right]g_{ij} \tag{11}$$

For unsteady case (1), the equation with variable coefficients will be similar to (2), but the coefficients c and d are functions of x, y and t; and the expression on the RHS becomes $g(x, y, t) - a[(\partial\phi)/(\partial t)]$. Using this we can obtain the semi-discrete form of the unsteady equation (1) using HOC as

$$\begin{aligned} &a\left[1 + \frac{h^2}{12}(\delta_x^2 - c_{ij}\delta_x) + \frac{k^2}{12}(\delta_y^2 - d_{ij}\delta_y)\right]\delta_t\phi_{ij} = \\ &\alpha_{ij}\delta_x^2\phi_{ij} + \beta_{ij}\delta_y^2\phi_{ij} - C_{ij}\delta_x\phi_{ij} + \left[\delta_x^2\delta_y^2 - c_{ij}\delta_x\delta_y^2 - d_{ij}\delta_x^2\delta_y - \gamma_{ij}\delta_x\delta_y\right]\phi_{ij} + G_{ij} \end{aligned} \tag{12}$$

This scheme can be used to solve any 2D unsteady transport equation using a suitable time integration technique along with proper boundary conditions. In this work Crank Nicholson scheme has been used for time integration. This makes our HOC scheme fourth-order accurate

in space and second-order accurate in time.

$$a\left[1+\frac{h^2}{12}(\delta_x^2-c_{ij}\delta_x)+\frac{k^2}{12}(\delta_y^2-d_{ij}\delta_y)\right]\delta_t^+\phi_{ij}^n=\frac{1}{2}\left(H_{ij}^n+H_{ij}^{n+1}\right) \tag{13}$$

where δ_t^+ denotes the forward difference operator and the superscript n stands for the time level. H_{ij}^n is given as

$$H_{ij}^n=\alpha_{ij}\delta_x^2\phi_{ij}^n+\beta_{ij}\delta_y^2\phi_{ij}^n-C_{ij}\delta_x\phi_{ij}^n+\frac{h^2+k^2}{12}\left[\delta_x^2\delta_y^2-c_{ij}\delta_x\delta_y^2-d_{ij}\delta_x^2\delta_y-\gamma_{ij}\delta_x\delta_y\right]\phi_{ij}^n+G_{ij}^n \tag{14}$$

3 Code Validation

The above HOC formulation (13) can be used to solve streamfunction-vorticity form of the 2D Navior-Stokes given by

$$-\nabla^2\psi=\omega \tag{15}$$

$$\frac{\partial\omega}{\partial t}+u\frac{\partial\omega}{\partial x}+v\frac{\partial\omega}{\partial y}=\frac{1}{Re}\nabla^2\omega \tag{16}$$

where ψ stands for streamfunction and ω for vorticity. The velocities in $x-$ and $y-$directions are given by

$$u=\psi_y \tag{17}$$

$$v=-\psi_x \tag{18}$$

To lend credibility to the present HOC code its results for single lid-driven square cavity flow (Fig. 1(a)) are compared with the results of Ghia et al. [13] at various Re's at grids 51 X 51, 71 X 71 and 101 X 101. Fourth-order compact approximations for velocities obtained from equations (16)-(18) are given by

$$u_{ij}=\delta_y\psi_{ij}+\frac{h^2}{6}\left(\delta_y\omega_{ij}+\delta_x^2\delta_y\psi_{ij}\right)+O(h^4) \tag{19}$$

$$v_{ij}=-\delta_x\psi_{ij}-\frac{h^2}{6}\left(\delta_x\omega_{ij}+\delta_x\delta_y^2\psi_{ij}\right)+O(h^4) \tag{20}$$

The value of the streamfunction ψ is taken to be zero on all the boundaries while the Neumann boundary condition for vorticity is derived using a fourth-order compact scheme. For example, on the leftmost wall ($x=0, 0\le y\le 1$), the approximation for ω can be found from the relation $v=-\psi_x$ and equations (15) and (16) to get

$$-\delta_x^+\psi_{0j}-\left[\frac{h}{2}+\frac{h^2}{6}\delta_x^+-\frac{h^3}{24}\left(Rev_{0j}\delta_y-\delta_y^2\right)\right]\omega_{0j}=v_{0j}-\frac{h^3}{24}\left(\delta_x^+\delta_y v_{0j}-\delta_t\omega_{0j}\right) \tag{21}$$

where the suffixes 0 and j stand for the leftmost wall and the vertical space index respectively. Using the boundary conditions for left wall, i.e., $v_{0j}=0$ and $\psi_{0j}=0$, the vorticity at the left wall can be explicitly written as

$$\omega_{0j}^{n+1}=\frac{24\Delta t}{h^3}\left[-\frac{\psi_{1j}^n}{h}-\frac{h}{2}\omega_{0j}^n-\frac{h}{6}\left(\omega_{1j}^n-\omega_{0j}^n\right)-\frac{h}{24}\left(\omega_{0j+1}^n-2\omega_{0j}^n+\omega_{0j-1}^n\right)\right]+\omega_{0j}^n \tag{22}$$

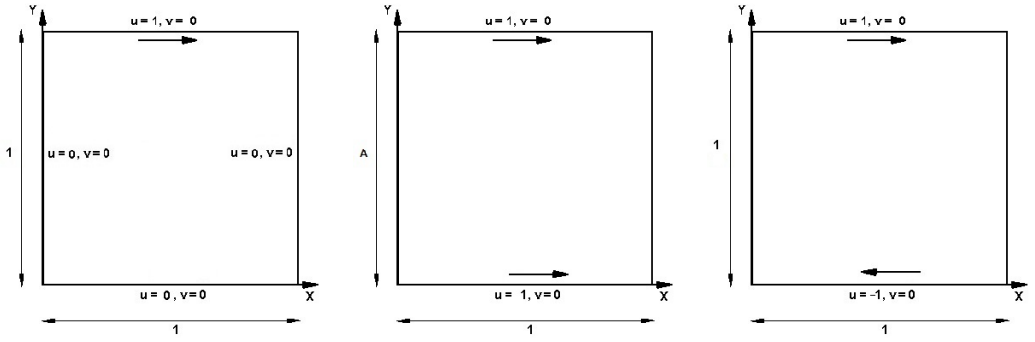

(a) Single lid-driven Cavity (b) Two-sided lid-driven cavity (parallel motion of facing walls) (c) Two-sided lid-driven cavity (antiparallel motion of facing walls)

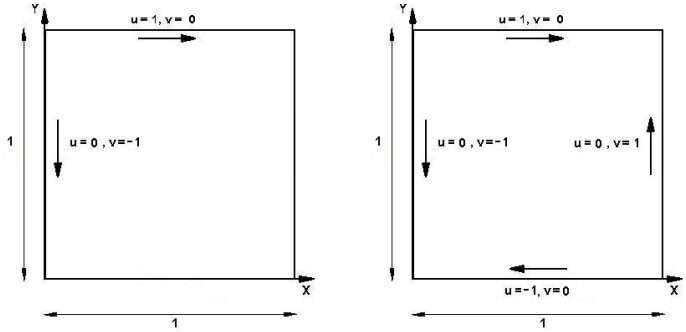

(d) Two-sided lid-driven cavity (motion of non-facing walls) (e) Four-sided lid-driven cavity

Figure 1: Geometry and boundary conditions for cavities considered in this work.

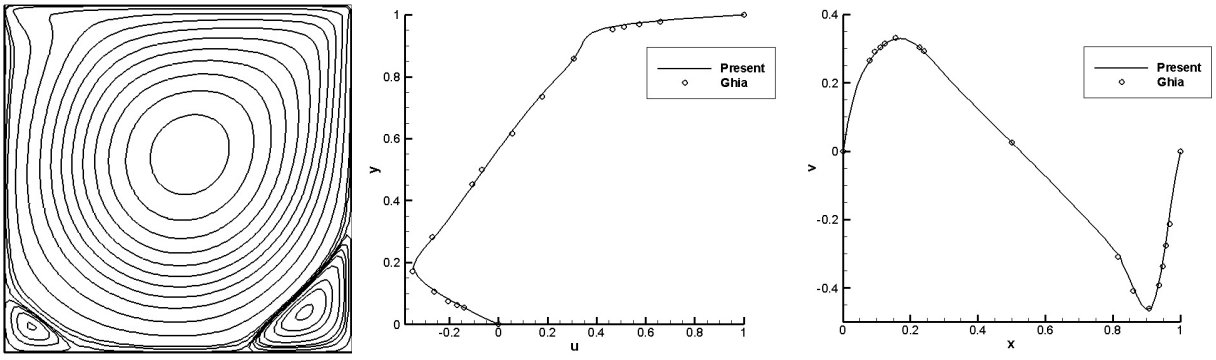

(a) Streamlines (b) u velocity along vertical centreline (c) v velocity along horizontal centreline

Figure 2: Code validation: single lid-driven square-cavity ($Re = 1000$).

The boundary conditions for the other walls can be derived in a similar manner.

For corners it is not possible to obtain fourth-order expressions of vorticity due to geometry constraints. Hence we use a third-order approximation. For example, for the upper left corner (x_0, y_{N-1}), vorticity can be written by approximating equations (17) and (18) in both $x-$ and $y-$directions and approximating the higher-order terms appropriately. This results in

$$\left[\frac{h}{2} + \frac{h^2}{6}\left(\delta_x^+ - \delta_y^-\right)\right]\omega_{0,N-1} = -\left[\delta_x^+ + \delta_y^-\right]\psi_{0,N-1} - u_{0,N-1} - v_{0,N-1}$$

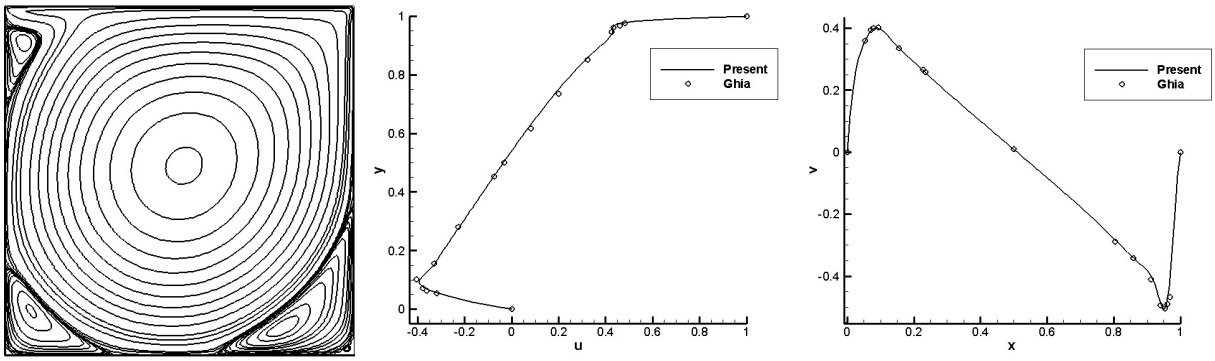

(a) Streamlines (b) u velocity along vertical centreline (c) v velocity along horizontal centreline

Figure 3: Code validation: single lid-driven square-cavity ($Re = 5000$).

$$-\frac{h^2}{6}\left[\delta_x^+\delta_y^- u_{0,N-1} + \delta_x^+\delta_y^- v_{0,N-1}\right] + O(h^3) \tag{23}$$

where the suffix $N-1$ denotes all the points lying on $y = 1$. The boundary conditions for other corners can be written in a similar manner. The procedure for boundary conditions is outlined in [18].

The results presented here are on a 101 X 101 grid for Re's 1000 and 5000 (Figs. 2 and 3). The obtained results are in very good agreement even for a relatively high Reynolds number ($Re = 5000$) on a coarse grid of 101 X 101. This shows the higher-order nature of the scheme. Thus the present HOC code stands validated.

4 Results and Discussion

4.1 Two-sided cavity - Motion of facing walls

Figs. 1(b) and 1(c) show the two-sided cavity with parallel and antiparallel motion of facing walls respectively. All computations are performed at $Re = 600$ for parallel wall motion of rectangular cavity (Fig. 1(b)). Multiple solutions are obtained when $A \geq 0.556$. This value is in good agreement to the previously reported value of 0.559 [2]. Fig. 4 shows the multiple solutions obtained at $A = 0.65$. It is observed that one symmetric and a pair of asymmetric solutions exist at this aspect ratio. However at $A = 0.875$, an extra pair of weakly asymmetric solutions can also be seen to exist. Thus a total of five solutions exist for $A = 0.875$. These are shown in Fig. 5.

Computations are also carried out at various Re's for parallel motion of a square cavity (Fig. 1(b) with $A = 1$). It is seen that a total of three solutions exist for $Re \geq 983.5$. This threshold value is again in good agreement with previously investigations [2, 6]. Fig. 6 shows multiple solutions at $Re = 3500$ for this configuration.

For antiparallel motion of facing walls in a square cavity (Fig. 1(c)), multiple solutions are seen for $Re \geq 3203$ [12]. Below this Re value, the additional solutions merge to form a single solution. Fig. 7 shows the multiple solutions at $Re = 3300$.

4.2 Two-sided cavity - Motion of non-facing walls

Using the same HOC scheme, an attempt is now made to re-examine the existence of multiple solutions for motion of non-facing walls of a square cavity. Existing literature has shown that a total of three solutions exist above a critical Re value of 1071 [8]. In this work, we show that

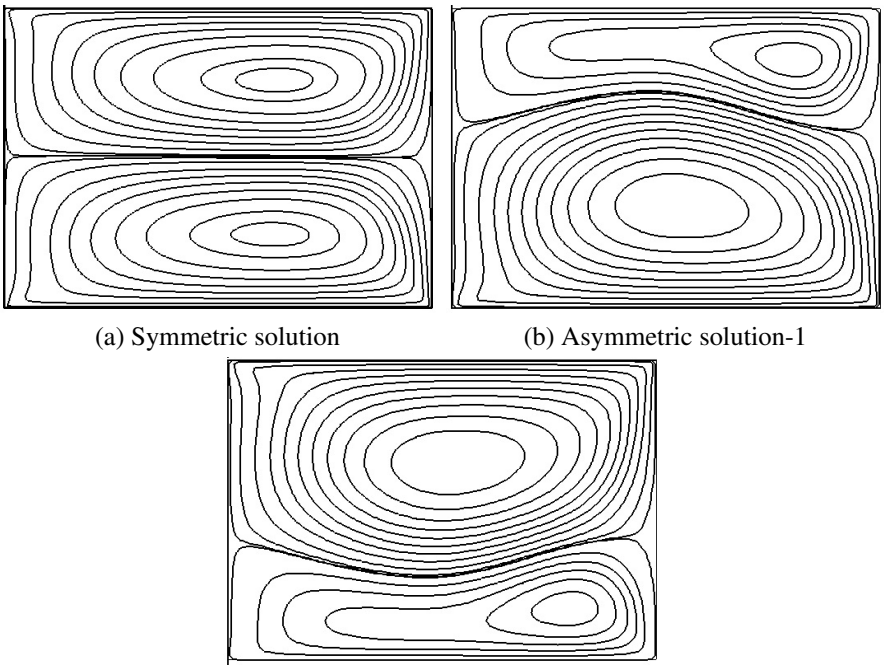

(a) Symmetric solution (b) Asymmetric solution-1

(c) Asymmetric solution-2

Figure 4: Multiple solutions of parallel wall motion for $A = 0.65$ at $Re = 600$.

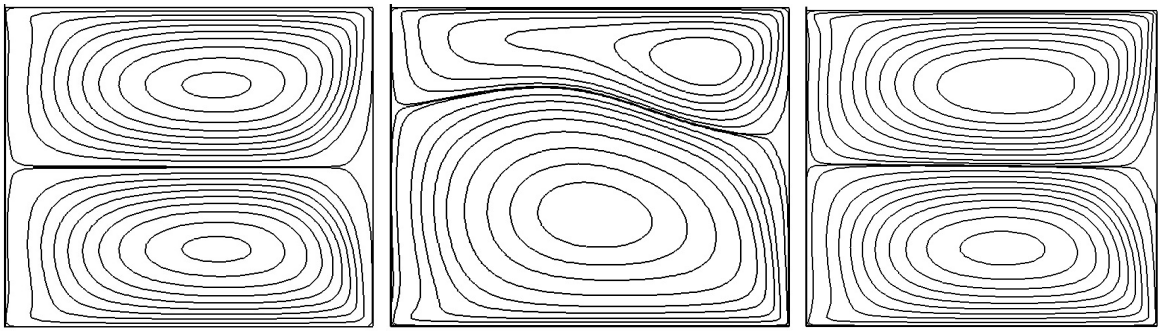

(a) Symmetric solution (b) Asymmetric solution (c) Weakly asymmetric solution

Figure 5: 3 out of 5 multiple solutions of parallel wall motion for $A = 0.875$ at $Re = 600$.

these extra solutions can be obtained at a significantly lower Re value of 975. Figs. 8 and 9 show multiples solutions at $Re = 975$ and 2000 respectively. It may be noted that $\psi = 0$ along the main diagonal for the solutions shown in Figs. 8(a) and 9(a).

4.3 Four-sided cavity

The geometric configuration for four-sided cavity flow is given in Fig. 1(e). Wahba [8] obtained a threshold value of $Re = 129$ above which multiplicity of solutions was obtained. Using the HOC scheme (13), multiple solutions are seen for $Re \geq 130$. For $Re < 130$, only a single symmetric solution can be obtained. Figs. 10 and 11 show all the multiple solutions obtained at $Re = 150$ and 300 respectively.

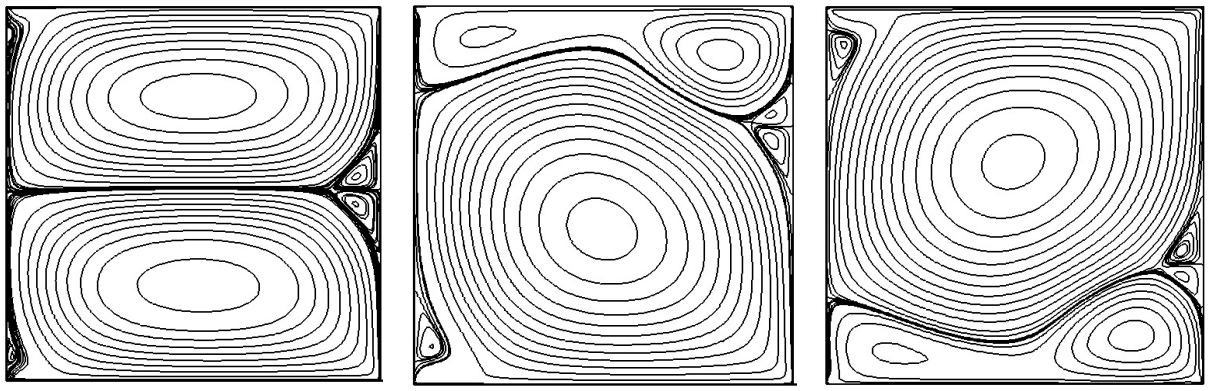

(a) Symmetric solution (b) Asymmetric solution 1 (c) Asymmetric solution 2

Figure 6: All solutions at $Re = 3500$ for parallel lid motion in a square cavity (Grid: 101 X 101).

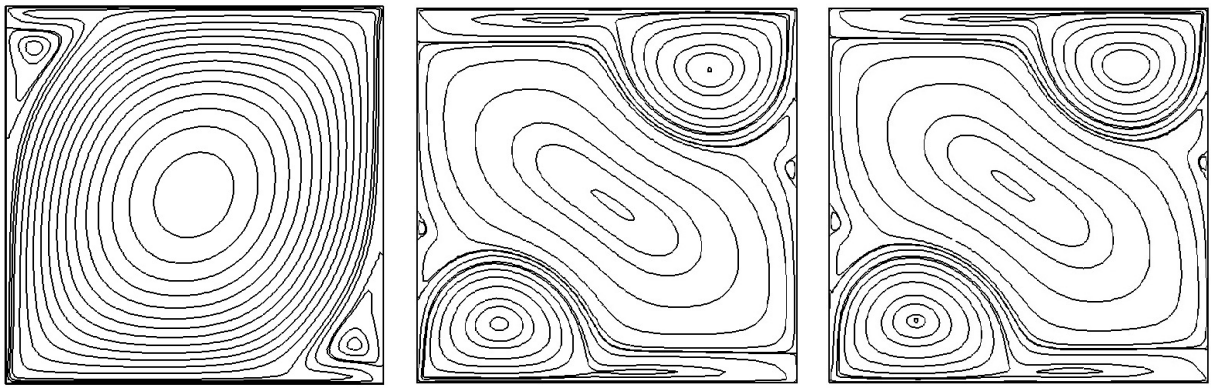

(a) Symmetric (b) Asymmetric 1 (c) Asymmetric 2

Figure 7: All solutions at $Re = 3300$ for antiparallel lid motion in a square cavity (Grid: 101 X 101).

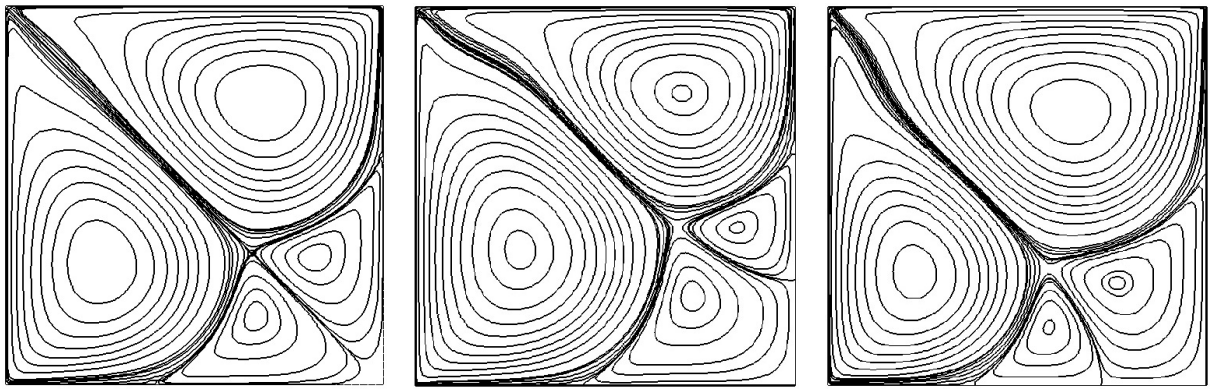

(a) Symmetric solution (b) Asymmetric solution 1 (c) Asymmetric solution 2

Figure 8: All solutions at $Re = 975$ for motion of non-facing walls in a square cavity (Grid: 101 X 101).

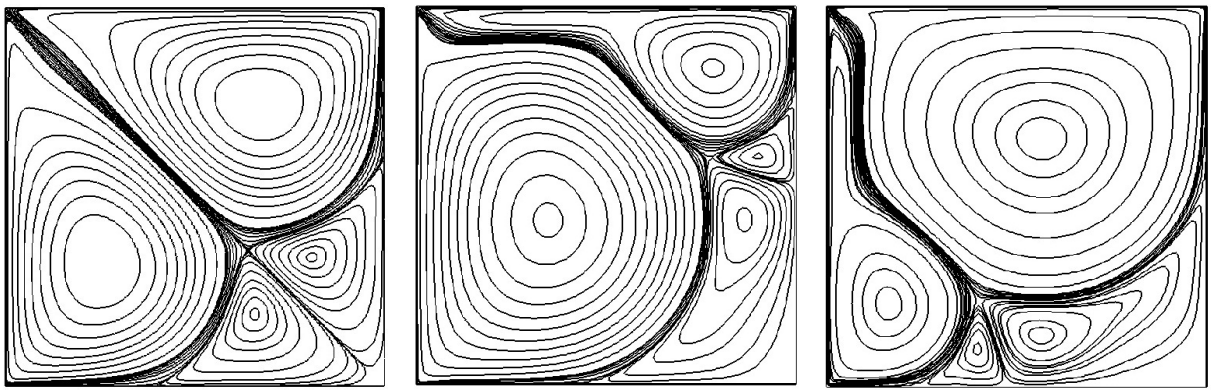

(a) Symmetric solution (b) Asymmetric solution 1 (c) Asymmetric solution 2

Figure 9: All solutions at $Re = 2000$ for motion of non-facing walls in a square cavity (Grid: 101 X 101).

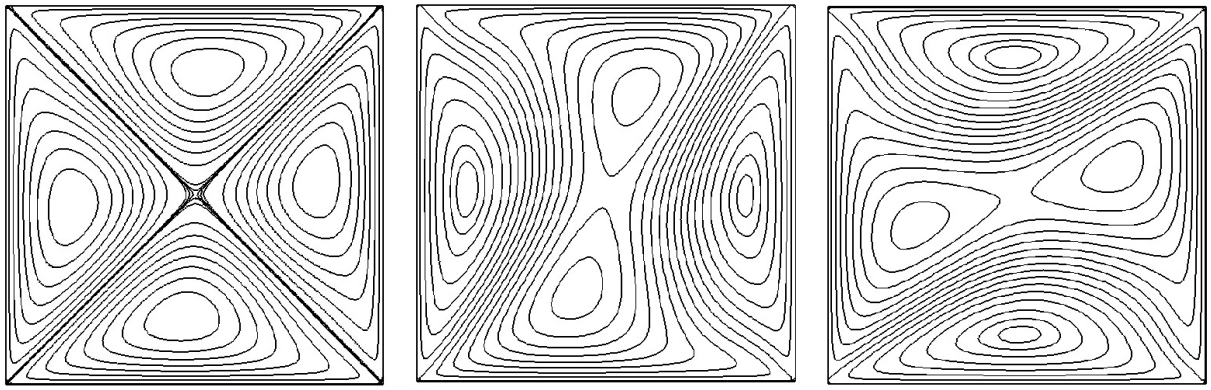

(a) Symmetric solution (b) Asymmetric solution 1 (c) Asymmetric solution 2

Figure 10: All solutions at $Re = 150$ for four-sided square cavity (Grid: 101 X 101).

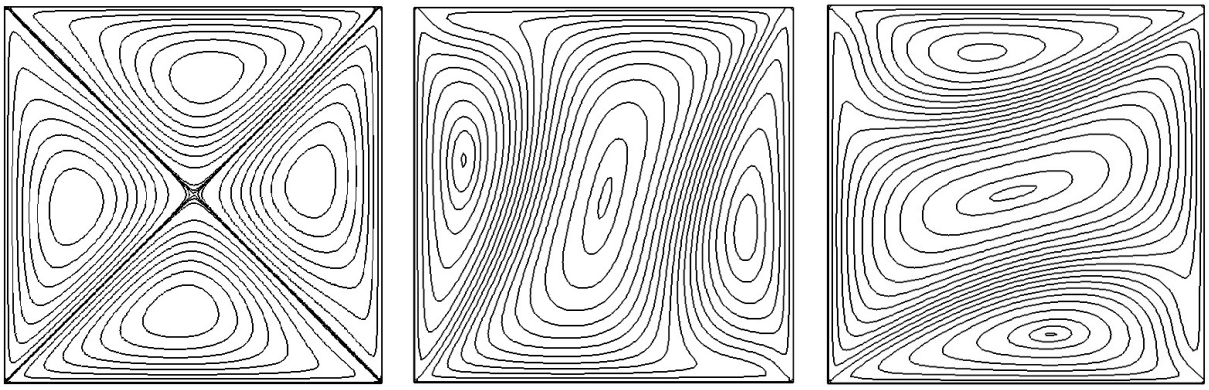

(a) Symmetric solution (b) Asymmetric solution 1 (c) Asymmetric solution 2

Figure 11: All solutions at $Re = 300$ for four-sided square cavity (Grid: 101 X 101).

Table 1: Comparison of current computation with previous investigations

Cavity Configuration	Threshold Parameter	
	HOC	non-compact
Two-sided rectangular cavity with parallel facing wall motion ($Re = 600$)	$A \geq 0.556$	$A \geq 0.559$ [2]
Two-sided square cavity with parallel facing wall motion	$Re \geq 983.5$	$Re \geq 980$ [6] $Re \geq 990$ [2]
Two-sided square cavity with antiparallel facing wall motion	$Re \geq 3203$	-
Two-sided square cavity with non-facing wall motion	$Re \geq 975$	$Re \geq 1071$ [8]
Four-sided square cavity	$Re \geq 130$	$Re \geq 129$ [8]

5 Conclusion

A higher-order compact scheme of fourth-order spatial and second-order temporal accuracy is used to examine multiple stable steady-state solutions for both two-sided and four-sided cavity flows. For two-sided cavity flows with parallel motion of facing walls at $Re = 600$, three to five multiple steady solutions are obtained depending on the cavity aspect ratio. These solutions consist of a symmetric solution and one or two pairs of asymmetric solutions. It is seen that multiple solutions do not exist and only the symmetric solution exists for the movement of the longer plate below an aspect ratio of 0.556. For parallel lid motion of facing walls in a square cavity (when aspect ratio equals one) only symmetric solutions exist below $Re = 983.5$. The threshold values, of aspect ratio for rectangular and Re for square cavities, are carefully computed and they are close to those obtained in earlier investigations. Multiple solutions are also presented for antiparallel of facing walls in a square cavity. For two-sided cavity flows with motion of non-facing walls, we establish the existence of multiple solutions at $Re = 975$, which is significantly below the previously known threshold value of 1071. An exhaustive grid independence exercise was undertaken in order to obtain this threshold value. Multiple solutions are computed for four-sided square cavity flows as well. The critical Re value above which the multiple solutions exist in this configuration is in good agreement with previous investigations. It is well known that many nonlinear flow problems exhibit multiple solutions and this work demonstrates the ability of HOC schemes to obtain such solutions that violate the desirable mathematical condition of well-posedness.

References

[1] Perumal DA, Dass AK. Multiplicity of steady solutions in two-dimensional lid-driven cavity flows by lattice boltzmann method. *Computers & Mathematics with Applications* 2011; **61**(12):3711–3721.

[2] Albensoeder S, Kuhlmann H, Rath H. Multiplicity of steady two-dimensional flows in two-sided lid-driven cavities. *Theoretical and Computational Fluid Dynamics* 2001; **14**(4):223–241.

[3] Kuhlmann H, Wanschura M, Rath H. Elliptic instability in two-sided lid-driven cavity flow. *European Journal of Mechanics-B/Fluids* 1998; **17**(4):561–569.

[4] Kuhlmann H, Wanschura M, Rath H. Flow in two-sided lid-driven cavities: non-uniqueness, instabilities, and cellular structures. *Journal of Fluid Mechanics* 1997; **336**:267–299.

[5] Bruneau CH, Saad M. The 2d lid-driven cavity problem revisited. *Computers & Fluids* 2006; **35**(3):326–348.

[6] Lemée T, Kasperski G, Labrosse G, Narayanan R. Multiple stable solutions in the 2d symmetrical two-sided square lid-driven cavity. *Computers & Fluids* 2015; **119**:204–212.

[7] Peng YF, Shiau YH, Hwang RR. Transition in a 2-d lid-driven cavity flow. *Computers & Fluids* 2003; **32**(3):337–352.

[8] Wahba E. Multiplicity of states for two-sided and four-sided lid driven cavity flows. *Computers & Fluids* 2009; **38**(2):247–253.

[9] Blohm C, Kuhlmann HC. The two-sided lid-driven cavity: experiments on stationary and time-dependent flows. *Journal of Fluid Mechanics* 2002; **450**:67–95.

[10] Luo WJ, Yang RJ. Multiple fluid flow and heat transfer solutions in a two-sided lid-driven cavity. *International journal of heat and mass transfer* 2007; **50**(11):2394–2405.

[11] Kalita JC, Dalal D, Dass AK. A class of higher order compact schemes for the unsteady two-dimensional convection–diffusion equation with variable convection coefficients. *International Journal for Numerical Methods in Fluids* 2002; **38**(12):1111–1131.

[12] Prasad C, Dass AK. Use of an hoc scheme to determine the existence of multiple steady states in the antiparallel lid driven flow in a two-sided square cavity. *Computers & Fluids* 2016; **submitted for publication**.

[13] Ghia U, Ghia KN, Shin C. High-re solutions for incompressible flow using the navier-stokes equations and a multigrid method. *Journal of computational physics* 1982; **48**(3):387–411.

[14] Spotz WF, Carey G. *High-order compact finite difference methods with applications to viscous flows*. Citeseer, 1994.

[15] Abarbanel S, Kumar A. Compact high-order schemes for the euler equations. *Journal of Scientific Computing* 1988; **3**(3):275–288.

[16] Lele SK. Compact finite difference schemes with spectral-like resolution. *Journal of computational physics* 1992; **103**(1):16–42.

[17] Bassi F, Rebay S. A high-order accurate discontinuous finite element method for the numerical solution of the compressible navier–stokes equations. *Journal of computational physics* 1997; **131**(2):267–279.

[18] Spotz W, Carey G. High-order compact scheme for the steady stream-function vorticity equations. *International Journal for Numerical Methods in Engineering* 1995; **38**(20):3497–3512.